Massively parallel sequencing identifies the gene *Megf8* with ENU-induced mutation causing heterotaxy

Zhen Zhang[a], Deanne Alpert[a], Richard Francis[a], Bishwanath Chatterjee[a], Qing Yu[a], Terry Tansey[a], Steven L. Sabol[a], Cheng Cui[a], Yongli Bai[b], Maxim Koriabine[b], Yuko Yoshinaga[b], Jan-Fang Cheng[c], Feng Chen[c], Joel Martin[c], Wendy Schackwitz[c], Teresa M. Gunn[d], Kenneth L. Kramer[a], Pieter J. De Jong[b], Len A. Pennacchio[c], and Cecilia W. Lo[a,1]

[a]Laboratory of Developmental Biology, National Heart Lung and Blood Institute, Bethesda, MD 20892-1583; [b]BACPAC Resources Center, Children's Hospital Oakland Research Institute, Oakland, CA 94609; [c]U.S. Department of Energy Joint Genome Institute, Walnut Creek, CA 94598; and [d]Department of Biomedical Sciences, Cornell University College of Veterinary Medicine, Ithaca, NY 14853

Communicated by Marshall Nirenberg, National Institutes of Health, Bethesda, MD, December 31, 2008 (received for review December 5, 2008)

Forward genetic screens with ENU (*N*-ethyl-*N*-nitrosourea) mutagenesis can facilitate gene discovery, but mutation identification is often difficult. We present the first study in which an ENU-induced mutation was identified by massively parallel DNA sequencing. This mutation causes heterotaxy and complex congenital heart defects and was mapped to a 2.2-Mb interval on mouse chromosome 7. Massively parallel sequencing of the entire 2.2-Mb interval identified 2 single-base substitutions, one in an intergenic region and a second causing replacement of a highly conserved cysteine with arginine (C193R) in the gene *Megf8*. *Megf8* is evolutionarily conserved from human to fruit fly, and is observed to be ubiquitously expressed. Morpholino knockdown of *Megf8* in zebrafish embryos resulted in a high incidence of heterotaxy, indicating a conserved role in laterality specification. *Megf8*^{C193R} mouse mutants show normal breaking of symmetry at the node, but Nodal signaling failed to be propagated to the left lateral plate mesoderm. Videomicroscopy showed nodal cilia motility, which is required for left–right patterning, is unaffected. Although this protein is predicted to have receptor function based on its amino acid sequence, surprisingly confocal imaging showed it is translocated into the nucleus, where it is colocalized with Gfi1b and Baf60C, two proteins involved in chromatin remodeling. Overall, through the recovery of an ENU-induced mutation, we uncovered *Megf8* as an essential regulator of left–right patterning.

cardiogenesis | left–right | nodal

The power of forward genetic screens is well illustrated by the remarkable success of the *Drosophila* chemical mutagenesis screen used to dissect the genetic pathways specifying the segmental body plan (1). This study elegantly showed the efficacy of phenotype driven mutagenesis screens in the systematic analysis of complex biological processes regulating developmental patterning. To elucidate the genetic basis for congenital heart disease, we pursued a high throughput mouse ENU mutagenesis screen using noninvasive fetal echocardiography for cardiovascular phenotyping. ENU is a potent mutagen ideally suited for the production of human disease models in mice, because it predominantly generates point mutations, which are often associated with human diseases. More than 13,000 mouse fetuses were ultrasound interrogated, with 4% of the fetuses showing some evidence of cardiac defects (2, 3). This highly efficient cardiovascular phenotyping protocol suggests the possibility of a saturation mutagenesis screen.

The recovery of ENU-induced mutations in mice traditionally entails breeding the mutation generated in one inbred strain into a different inbred strain background, thereby allowing the use of polymorphic DNA markers to map the mutation. Genome scanning of many meiotic recombinants with such polymorphic DNA markers can eventually reduce the map interval to <1 Mb, when sequencing of candidate genes becomes more practical. This traditional approach for mutation recovery is costly and time consuming, and the mutation may be missed in regions with incomplete genome annotation. However, with rapid advances in a new generation of high throughput DNA sequencing technologies (4–6), rapid and low cost sequencing may greatly facilitate mutation recovery from mutagenesis screens. These new sequencing technologies have already proven useful for addressing a wide range of biological questions, from de novo sequencing of microorganisms (7), cancer mutation discovery (8), gene expression profiling (9) to epigenetic regulation (10).

In this study, we used massively parallel sequencing to recover an ENU-induced mutation causing a single-ventricle spectrum of complex structural heart defects recovered in our mouse fetal echocardiography screen (11). This mutant exhibits transposition of the great arteries, randomized left–right cardiopulmonary and visceral organ situs, a constellation of phenotype referred to as heterotaxy. This mutant also exhibits preaxial polydactyly. We mapped this mutation to a 2.2-Mb interval on mouse chromosome 7. Massively parallel DNA sequencing of the entire 2.2-Mb critical region revealed the underlying genetic lesion as a point mutation in a highly conserved gene, *Megf8*. *Megf8* is expressed ubiquitously, and plays an essential role in left–right patterning through the regulation of Nodal signaling. Overall, through the recovery of an ENU-induced mutation, we uncovered *Megf8* as an essential regulator of left–right patterning.

Results

Recovery of *Megf8* Mutation. A recessive mutation was previously recovered exhibiting a single-ventricle spectrum of complex congenital heart defects associated with heterotaxy. Typically these mutants exhibited thoracoabdominal organ situs anomalies that included dextracardia/mesocardia, right pulmonary isomerism, transposition of the great arteries, abnormal pulmonary venous connections, right-sided stomach and asplenia/polysplenia (Fig. S1 *A–C*) (11). We reported the mapping of this mutation to a 3.3-Mb interval on mouse chromosome 7. With analysis of a total of 142 meiotic recombinants, we narrowed the map interval to a 2.2-Mb critical region between markers D7Mit192-SNP rs13460395 (Table S1). Exon sequencing of a number of potential candidates showed no mutation. Because the mapped genomic interval is gene dense, systematic resequencing of all coding exons was impractical.

To examine the feasibility of using massively parallel DNA sequencing to recover the mutation in this genomic interval, we

Author contributions: P.J.D.J., L.A.P., and C.W.L. designed research; Z.Z., D.A., R.F., B.C., Q.Y., T.T., S.L.S., C.C., Y.B., M.K., Y.Y., J.-F.C., F.C., J.M., W.S., K.L.K., and C.W.L. performed research; T.M.G. contributed new reagents/analytic tools; Z.Z., D.A., R.F., B.C., Q.Y., T.T., S.L.S., C.C., Y.B., M.K., Y.Y., J.-F.C., F.C., J.M., W.S., K.L.K., P.J.D.J., L.A.P., and C.W.L. analyzed data; and Z.Z. and C.W.L. wrote the paper.

The authors declare no conflict of interest.

[1]To whom correspondence should be addressed. E-mail: loc@nhlbi.nih.gov.

This article contains supporting information online at www.pnas.org/cgi/content/full/0813400106/DCSupplemental.

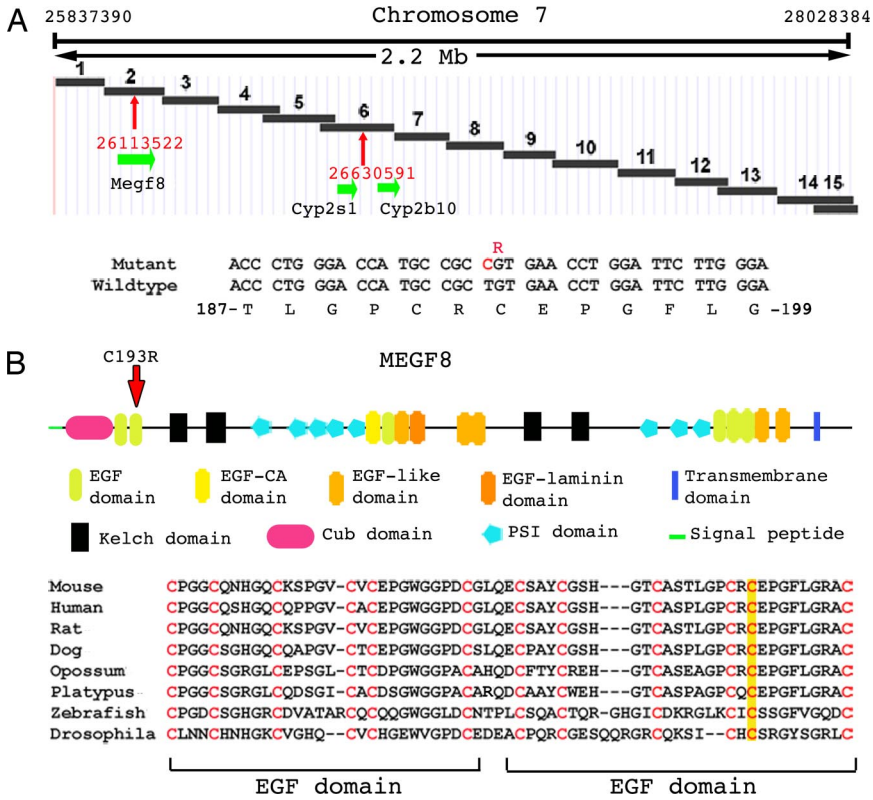

Fig. 1. Recovery of *Megf8* Mutation (*A*). A 15 BAC contig was obtained spanning the 2.2-Mb critical region containing the mutation in chromosome 7 (25, 837,390–28,028,384 b, NCBI m37 assembly). Sequencing showed a T to C substitution, causing cysteine (C) to arginine (R) amino acid replacement in *Megf8*, and another C to A substitution in a noncoding intergenic region. (*B*) *Megf8* encodes a protein containing EGF, EGF-calcium, EGF-like, EGF-laminin, kelch, plexin, and CUB domains, with the C193R substitution situated in the second conserved EGF domain. The mutated cysteine is highlighted in the comparative sequence alignment.

constructed a BAC library containing genomic DNA from the mutant and assembled a 10-fold redundant BAC contig spanning the 2.2-Mb critical region (Fig. S2). From this BAC contig, a minimum tiling path of 15 BACs was delineated (Fig. 1*A* and Fig. S2). These were pooled and sequenced with 70-fold coverage by massively parallel sequencing. A total of 303 Mb of sequences were generated. Reads were aligned using BLAT to the C57BL/6J reference sequence, the strain background in which the mutation was generated, and potential SNPs were identified as mismatches within the alignments. Filtering for a minimum depth of 5 reads and at least 70% of aligned reads containing the mismatch identified 10 putative variants. All 10 putative mutations were independently assessed by Sanger sequencing, with 2 (26113522 and 26630591) subsequently being sequence confirmed. One mutation was a single base change of a C to A in a non conserved intergenic region, and a second T to C substitution was identified causing a missense mutation (C193R) in the gene *Megf8* (Fig. 1*A*).

The point mutation in the intergenic region resides in a repetitive element that is not conserved, even between mouse and rat. Hence, this intergenic mutation is unlikely to be deleterious. In contrast, *Megf8* encodes a well-conserved protein of 2,789 aa (GenBank EU723517). Orthologs are found in many other species, including human, zebrafish and *Drosophila* (Fig. 1*B*). The SMART domain tool (12) predicts Megf8 contains multiple EGF, EGF-like, calcium-binding EGF-like and laminin-type EGF-like repeats, kelch domains, plexin repeats, and a CUB and transmembrane domain (Fig. 1*B*). The missense mutation eliminates an invariant cysteine situated in the second putative EGF domain, and could disrupt formation of a disulfide bond required for proper protein folding. Thus, this second mutation is a good candidate as the genetic lesion causing the defect phenotype in this mutant line. Consistent with this, the systematic analysis of nearly 200 embryos showed the mutant phenotype was strictly associated with the 42 homozygote $Megf8^{C193R}$ ($Megf8^{m/m}$) mutant embryos.

***Megf8* Morpholino Knockdown in Zebrafish Causes Heterotaxy.** To evaluate the biological function of *Megf8*, we carried out morpholino knockdown in zebrafish embryos. *Megf8* knockdown recapitulated the heterotaxy phenotype of $Megf8^{m/m}$ mutants, with discordant heart and gut situs observed in 75% of zebrafish *Megf8* morphants (Fig. 2*I* and Tables S2 and S3). Among the zebrafish embryos with discordant situs, 10% showed reverse heart looping, and 59% had abnormal or no looping. The latter embryos often exhibited a shortened heart tube (Fig. 2*C*), indicative of a role for *Megf8* in cardiac morphogenesis (11). Approximately half of the embryos with abnormal heart looping showed reverse looping of the gut. This same constellation of situs defects was observed with 2 independent splice-blocking morpholinos (Fig. S3). These results confirm *Megf8* is indispensable for left–right patterning. The recapitulation of the mouse heterotaxy phenotype with *Megf8* morpholino knockdown would suggest this C193R mutation might be a loss of function mutation.

Nodal Signaling Fails to Propagate to the Left LPM. To investigate the developmental origin of laterality defects in the $Megf8^{m/m}$ embryos, we examined the direction of embryonic turning and heart looping, two early indicators of left–right specification. $Megf8^{m/m}$

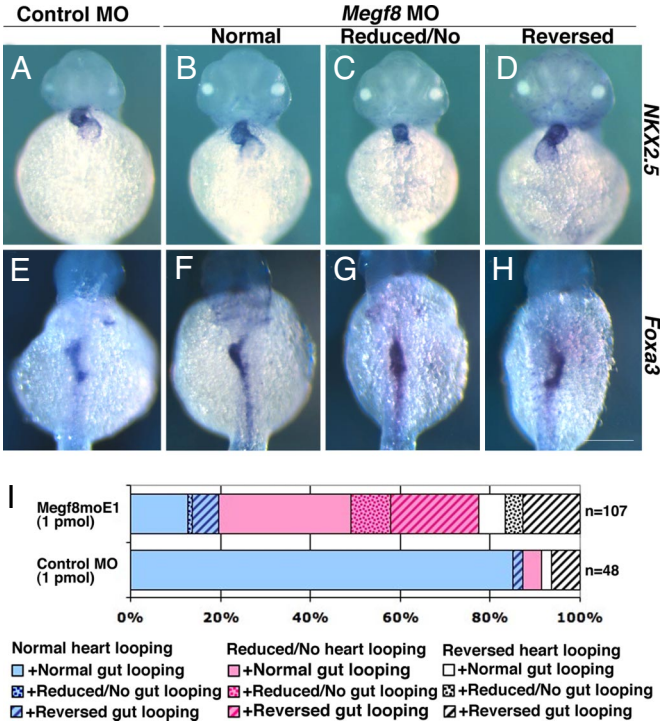

Fig. 2. Morpholino knockdown of *Megf8* causes situs discordance of heart tube and foregut. Zebrafish embryos injected with control or *Megf8* morpholinos were examined for heart and gut situs defects using RNA in situ hybridization analysis with *Nkx2.5* (*A–D*) and *Foxa3* (*E–H*) probes to visualize the heart tube and gut, respectively. In the majority of zebrafish embryos injected with control morpholino, the heart tube exhibited normal rightward looping delineating a S-shaped heart tube (*A*), whereas the foregut showed normal leftward looping (*E*). *Megf8* morpholino injection resulted in randomization of the direction of looping for both the heart tube (*B–D*) and foregut (*F–H*). *Megf8* morphants show normal (*B* and *F*), reduced or no looping (*C* and *G*), or reversed looping (*D* and *H*). (*I*) The distribution of heart and foregut looping pattern observed in the control and *Megf8* morphants is summarized in the bar graph. Note that 74% of *Megf8* morphants show heterotaxy, as indicated by discordance in their heart and gut situs. (*A–D*) Embryos shown in ventral view with anterior at the top. (*E–H*) Embryos shown in ventral view with anterior at the top. (Scale bar: 100 μm.)

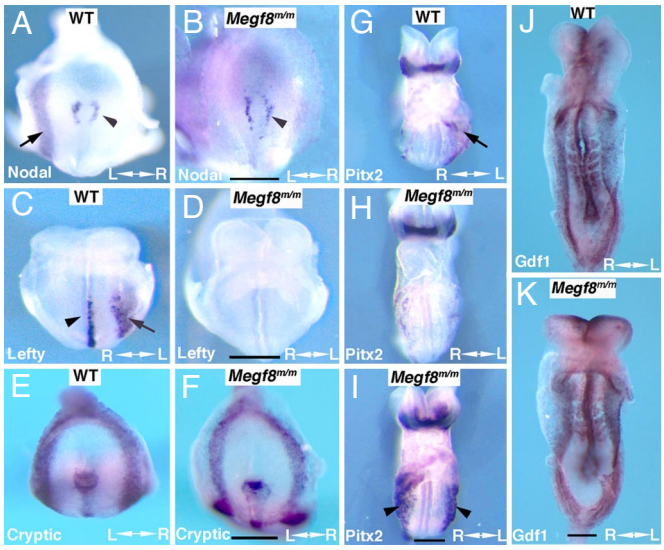

Fig. 3. In situ hybridization analysis show altered expression of left determinant genes in *Megf8*$^{m/m}$ embryos. (*A* and *B*) *Nodal* is expressed at the node (arrowhead) and in the left LPM (arrow) in 4 somite stage wild-type embryo (*A*). In *Megf8*$^{m/m}$ embryos, Nodal expression was preserved at the node (arrowhead), but absent in the LPM. (*C* and *D*) In wild-type embryos, *Lefty1* and *2* are normally expressed in the floor plate (arrowhead) and left LPM (arrow), respectively (*C*), but, in *Megf8*$^{m/m}$ mutants, expression of both *Lefty 1* and *2* are lost (*D*). (*E* and *F*) *Cryptic* expression in the node and LPM show no change in *Megf8*$^{m/m}$ mutants (*F*) vs. wild-type (*E*) embryos. (*G–I*). Wildtype embryos show *Pitx2* expression in the left LPM (arrow in *G*), but this is either lost (*H*) or bilateral (arrowheads in *I*) in *Megf8*$^{m/m}$ mutant embryos. *Pitx2* expression in the head mesenchyme is unchanged. (*J* and *K*). *Gdf1* expression in the node and LPM is not affected in *Megf8*$^{m/m}$ (*K*) vs. wild-type (*J*) embryos. (*A*, *B*, *E*, and *F*) Dorsal view. (*C*, *D*, and *G–J*) Ventral view. WT, wild-type; left (L)–right (R) orientation indicated by double arrowheads. (Scale bar: 100 μm.)

embryos showed randomization in both embryonic turning and heart tube looping (Fig. S1 *D–H* and Table S4). We also noted an apparent shortening of the outflow tract, a phenotype reminiscent of the shortened heart tube seen in the zebrafish *Megf8* morphants (Fig. 2*C* and Fig. S1 *E* and *F*).

The breaking of symmetry and specification of left–right patterning are largely orchestrated by the embryonic expression of the highly conserved *Nodal*, *Lefty1*/*Lefy2* and *Pitx2* signaling network early in embryogenesis, largely spanning E7.75–8.5 (13). Notably, *Megf8* is not asymmetrically expressed, because RNA in situ hybridization analysis with 2 independent *Megf8* probes showed *Megf8* transcripts are ubiquitously expressed in the embryo (Fig. S4). This same pattern was observed in wild-type and *Megf8*$^{m/m}$ mutant embryo (Fig. S4). An early molecular evidence of left–right asymmetry is the transient asymmetry in *Nodal* expression at the embryonic node. Analysis of *Megf8*$^{m/m}$ mutants showed 3 of 7 embryos with stronger left sided perinodal expression of *Nodal* (Fig. 3*B*). This compared with 3 of 5 wild-type/heterozygous embryos exhibiting stronger left sided *Nodal* expression at the node (Fig. 3*A*). These results suggest the breaking of symmetry at the node is unaffected. Consistent with this, motile function associated with monocilia at the node, which is required for breaking symmetry (14), was also preserved (Fig. S5 and Quicktime Movie S1 and Movie S2).

Thus, *Megf8*$^{m/m}$ embryos exhibited normal clockwise ciliary rotation with a beat frequency indistinguishable from heterozygous and wild-type embryos. Using fluorescent beads, we also examined cilia generated flow at the node and again, no change was detected (Fig. S5). These findings suggest *Megf8* functions downstream of the node. Indeed, in situ hybridization analysis of *Megf8*$^{m/m}$ embryos showed *Nodal* expression, although intact at the node, was absent in the left LPM (n = 7, 3–4 somites) (Fig. 3*B*). Expression of genes downstream of *Nodal* was also disrupted, with *Lefty1* and *Lefty2* expression lost in the floor plate and LPM, respectively (n = 5, 4–5 somites, Fig. 3*D*). *Pitx2* expression in the LPM was either absent (n = 2) or bilateral (n = 5) (6–8 somites) (Fig. 3 *G–I*). In contrast, *Pitx2* expression in the head mesenchyme was unaffected.

Genetic analyses have suggested that *Nodal* expression at the node is required for the activation of left-determinant transcription cascade in the left LPM (15, 16). Our data, would suggest the molecular defect underlying the *Megf8*$^{m/m}$ phenotype is either an interruption of signal transfer from the node to left LPM and/or a disruption in the initiation and expansion of *Nodal* expression in the LPM. To further elucidate the underlying molecular mechanism, we examined the expression of *Gdf1* and *Cryptic*. *Gdf1* encodes a TGFβ superfamily ligand required for Nodal long-range action, including propagation of Nodal signaling from the embryonic node to the LPM (17), while Cryptic, a coreceptor required for Nodal signal reception, is also essential for *Nodal* expression in the left LPM (18). Knockout mutants of either gene have phenotypes that are very similar to the *Megf8*$^{m/m}$ mutants. However, in situ hybridization analysis showed no change in *Gdf1* and *Cryptic* expression in *Megf8*$^{m/m}$ mutants (Fig.

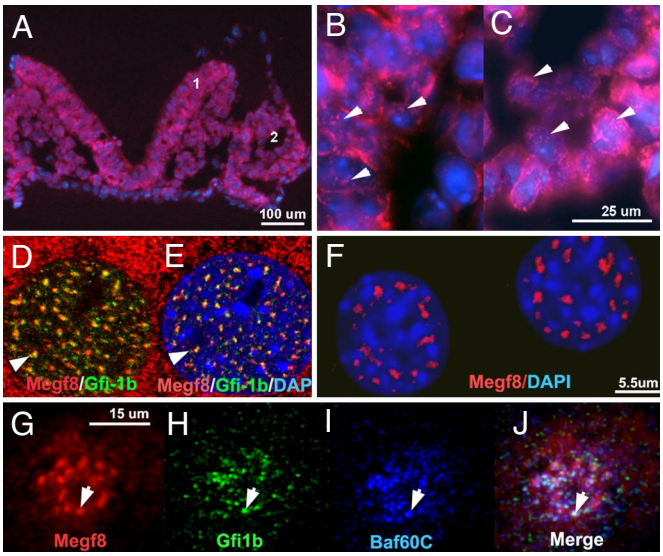

Fig. 4. Distribution of Megf8 in embryos and cultured cells. (*A–C*). Immunostaining with Megf8 antibody of an embryo at E8 show ubiquitous Megf8 expression. Regions 1 and 2 in *A* are enlarged in *B* and *C*. Punctate staining is observed in the nuclei (arrowheads in *B* and *C*), and there is also diffuse cytoplasmic staining. (*D–F*). Confocal imaging of MEFs (*D* and *E*) or NIH 3T3 (*F*) cells immnostainined with a Megf8 antibody show Megf8 distributed as punctate spots in the nuclei, largely in regions with low level DAPI staining. Coimmunostaining with Gfi1b antibody showed extensive colocalization of Megf8 with Gfi1b (*D* and *E*). (*G–J*). Confocal imaging of MEFs immunostained with antibodies to Megf8 (red), Gfi1b (green), and Baf60C (blue) showed some regions in the nucleus where all 3 proteins are colocalized in punctate spots (see arrowhead).

3 *E*, *F*, *J*, and *K*), suggesting *Megf8* regulation of Nodal signaling does not involve the modulation of *Gdf1* and *Cryptic* expression.

Punctate Nuclear Localization of Megf8. To further explore the possible function of *Megf8*, we generated an antibody to Megf8 to investigate its subcellular distribution. Although Megf8 is predicted to have a transmembrane domain, immunostaining and confocal imaging showed no cell surface localization in either mouse embryonic fibroblasts (MEFs) or NIH 3T3 cells. Instead, we observed prominent punctate nuclear staining and varying levels of cytoplasmic staining (Fig. 4 *D–F*). Immunostaining of embryo cryosections showed a similar distribution, including punctate nuclear localization (Fig. 4 *A–C*). No obvious change in Megf8 expression level or distribution was observed in either $Megf8^{m/m}$ embryos or MEFs derived from the mutant embryos (Fig. S6). The specificity of the Megf8 antibody was verified with *Megf8* siRNA knockdown, which largely abolished the Megf8 antibody staining (Fig. S6). In addition, Western immunoblotting of transfected cells expressing a C-terminal 3XFLAG-tagged Megf8 fusion protein gave an expected high molecular weight band that was detected by both the Megf8 and FLAG antibodies (Fig. S7).

The finding of Megf8 localization in the nucleus was particularly interesting in light of a previous report from a yeast 2-hybrid screen that identified Megf8 as a potential interacting partner of Gfi1b (19), a nuclear protein with known transcription repressor activity and a role in heterochromatinization in erythroid cell lineages (20, 21). Double immunostaining showed Megf8/Gfi1b are colocalized as punctate spots in the nucleus (Fig. 4 *D* and *E*). Unlike the localization seen in erythroid progenitors, in MEFs and NIH 3T3 cells, Gfi1b and Megf8 were not concentrated in heterochromatic regions delineated by strong DAPI staining (Fig. 4 *E* and *F*). Further analysis showed $Megf8^{m/m}$ mutants, unlike *Gfi1b* knockout mouse embryos (20), do not have defects in definitive erythropoeisis (Fig. S8). Conversely, *Gfi1b* knockout mouse embryos, unlike $Megf8^{m/m}$ mutants, did not exhibit laterality defects.

Interestingly, a chromatin remodeling protein, Baf60C, a component of the Swi/Snf-like BAF complex, also has been shown to play an essential role in left–right patterning, with the *Baf60C* knockdown mice exhibiting cardiac and laterality phenotypes very similar to the $Megf8^{m/m}$ mutants (22). Double immunostaining showed Megf8 and Baf60C have regions of overlapping localization in the nucleus. Triple immunostaining and confocal imaging with antibodies to Baf60C, Gfi1b, and Megf8 showed regions in which all 3 proteins are colocalized in the nucleus (Fig. 4 *G–J*). Together these findings suggest Megf8 may regulate Nodal signaling through a role in chromatin remodeling.

Discussion

Recovery of ENU-Induced Mutations by Massively Parallel Sequencing. Using massively parallel sequencing, we identified 2 single-base substitutions in a 2.2-Mb genomic interval containing an ENU-induced mutation causing heterotaxy. This is the first demonstration of the use of massively parallel sequencing in the recovery of ENU-induced mutations. We used a strategy combining both massively parallel sequencing and BAC contig construction to recover the ENU-induced mutations. This strategy obviated the presently prohibitive expense entailed in whole genome resequencing. By sequencing only a subset of the genome contained within the BAC contig, we also minimized potential complications from segmental duplications and repeat sequences in the mouse genome. Using BLAT analysis for sequence alignment, we obtained 10 mismatch calls in the 2.2-Mb genomic interval relative to the C57BL6J reference sequence, only 2 of which were corroborated as real mutations by Sanger sequencing. These results indicate refinement of the calling algorithms is needed before base calling for whole genome resequencing can be automated. Significant technical challenges also remain in the development of sequence alignment algorithms that can automate the assembly of short reads in whole genome sequencing projects when repeat sequences and segmental duplications are unavoidable.

We identified a single C to T base change (C193R) causing a cysteine to arginine substitution in the coding region of *Megf8*. In addition, a second C to A base change was found in a noncoding intergenic region in the mapped interval. These results are remarkably in line with previous estimate of one ENU-induced mutation per Mb, with one in 1.82 Mb expected to alter function (23). We note *Megf8* was not yet annotated in the mouse genome when this mutation was first mapped to mouse chromsome 7. Thus, a candidate gene sequencing strategy at that time would have failed to recover the mutation. We note with the recent emergence of sequence capture technology, targeted genome sequencing may be feasible without the expense entailed in BAC library construction (24, 25). Moreover, with the rapid decline in the cost of massively parallel sequencing, and the advent of real time single-molecule DNA sequencing technology (26), whole genome resequencing may be on the horizon, making the recovery of ENU-induced mutations affordable and straight forward.

Role of *Megf8* in Left–Right Patterning. Our studies show an essential role for *Megf8* in left–right patterning. Current model for left–right patterning suggests 4 discrete steps in left–right specification: first is the breaking of symmetry at the embryonic node, second is transfer of asymmetric signal from the node to the left LPM, third is Nodal-activated transcription of left-determinant genes such as *Pitx2* and *Lefty*, and 4th is the final asymmetric elaboration of organogenesis (13, 27). $Megf8^{m/m}$ mutants showed asymmetric expression of *Nodal* at the embryonic node, but neither *Nodal* nor *Lefty* was expressed

in the LPM, and *Pitx2* expression was either absent or bilateral. The discordance in *Pitx2* and *Nodal* expression in our mutant is reminiscent of previous studies showing the uncoupling of *Nodal* and *Pitx2* expression in zebrafish embryos (28) and in various mutant mouse models, such as the polycystin-2 knockout mice (29). It is interesting to note that polycystin-2, like *Megf8* is also ubiquitously expressed, and polycystin-2 knockout mutants show normal node expression of Nodal, but largely absent Nodal expression in the LPM. These findings suggest additional levels of complexities beyond the central Nodal signaling cascade in the specification of laterality. Overall, these findings show *Megf8* is required, not for the initial breaking of symmetry, but in subsequent steps to initiate *Nodal* expression in the left LPM.

The finding of prominent Megf8 colocalization with Gfi1b and Baf60C in the nucleus suggests a role in the regulation of gene expression in the left LPM through chromatin remodeling. Baf60c was shown to regulate left–right asymmetry through Notch-dependent transcription around the node (22). However, unlike *Baf60C* mutants, in situ hybridization showed no change in perinodal *Notch1* or *Delta1* expression in *Megf8*$^{m/m}$ mutants (Fig. S4), whereas *Baf60C* mutants, unlike *Megf8*$^{m/m}$ mutants, exhibit little or no expression of *Nodal* at the embryonic node. Because *Baf60c* is also expressed in the LPM, Baf60c and Megf8 could potentially act in the same chromatin remodeling complex to promote Nodal-driven asymmetric transcription in the LPM, either downstream of or in a pathway parallel to Notch-dependent regulation of left–right patterning.

Alternatively, Megf8 may regulate left–right patterning by facilitating the transfer of Nodal from the embryonic node to the left LPM. The long-range action of Nodal has been shown to require the formation of Nodal-Gdf1 heterodimers (17). Recent studies also suggest the interaction of Nodal and sulfated glycosaminoglycans (GAGs) play a role in the long-range propagation of Nodal signaling (30). The predicted protein structure of Megf8, which includes a transmembrane domain and many EGF repeats in the presumptive extracellular domain, would suggest it might function as a protein scaffold for GAGs or directly interact with Nodal or Gdf1 to stabilize Nodal-Gdf1 heterodimers. Although we failed to observe Megf8 immunolocalization at the cell surface, we cannot exclude a shorter Megf8 isoform being localized at the cell surface, because the Megf8 antibody was made using a peptide toward the N terminus. Similarly, it is possible that cleaved and secreted N-terminal Megf8 might play a role in Nodal-Gdf1 heterodimer transfer. Further studies are needed in the future to define the precise function of Megf8, including the analysis of conditional knockout mouse models to define the cell lineage requirement for Megf8 and its role in cardiac morphogenesis. Because *Megf8* mutants also exhibit preaxial polydactyly, it is possible that *Megf8* may have additional independent roles in other aspects of embryonic development.

Materials and Methods

Mutation Mapping. The mutation was mapped to a 3.3-Mb region of chromosome 7 between markers D7mit192 and D7mit266 (11). Further fine mapping was carried out using SNPs or microsatellite markers within the mapped interval that are polymorphic between C57BL/6J and C3H or A/J, and tracking the segregation of C57BL6 markers.

BAC Library Construction, Screening, and Sequencing. CHORI-602 BAC library construction was constructed as described in ref. 31. Briefly, DNA from a single homozygous mouse embryo was partially digested with EcoRI and cloned into the BAC vector pTARBAC2.1. Forty-four pairs of radiolabeled unique overlapping oligonucleotides (overgos) were used to screen the BAC library and172 BAC clones were identified as having genomic fragments in the critical region. Positive BAC clones were end-sequenced to locate genomic fragment boundary and 139 BACs were positively mapped to the critical region by end sequencing, and 15 overlapping BAC clones were identified comprising the minimal tiling path. Each BAC was independently isolated by standard alkaline lysis (Qiagen) and equimolar amounts of each BAC were pooled for standard Illumina Genome Analyzer I sequencing.

Videomicroscopy of Nodal Ciliary Motion. E7.5-E7.75 embryos were dissected and transferred node side down onto 35-mm glass-bottomed culture dishes. Videomicroscopy was carried out using a Leica DMIRE2 inverted microscope with a Phantom v4.2 camera (Vision Research). To quantify nodal flow, a small quantity of 0.20 μm Fluoresbrite microspheres (Polysciences) were added to the media bathing the node and fluorescent movies were collected using a cooled low light CCD camera (Hamamatsu; C9100-12). Volocity 3.5.1 software (Perkin–Elmer) was used to analyze speed and directionality of microsphere movement.

Zebrafish Morpholino Injections. Two antisense morpholino oligonucleotides (Megf8moE1 and Megf8moE2, Gene Tools) to *Megf8* were designed as illustrated in Fig. S3*A*. The standard negative control morpholino was provided by Gene Tools. Increasing doses (0.5 pmol to 4.0 pmol) were injected into 1-cell-stage embryos to determine optimal concentrations. At 48 h after fertilization, embryos were scored for the direction of heart looping or collected and fixed for in situ hybridization.

In Situ Hybridization Analysis. Whole mount RNA in situ hybridization was performed as described in ref. 32, using a robot (Intavis AG) with DIG-labeled probes for zebrafish *Nkx2.5* and *Foxa3*, and mouse *Nodal*, *Lefty1*, *Lefty2*, *Pitx2*, *Cryptic*, *Gdf1*, *Notch*, *and Delta2*. *Megf8* in situ hybridization probes were generated using PCR amplification with probe 1 generated using forward (5′CAACTACAGCGTCAACGGCAAC) and reverse (5′ TCACAGGCTCGTCCCAAGAATC) primers, and probe 2, with forward (5′ ACCCTTGAGCCCACAGAAGATG) and reverse (5′CGTGATAAGACAAACCGCTTCCAG) primers.

Immunostaining. Polyclonal antibody to Megf8 was raised in chickens by immunization with the synthetic peptide QQEKETRRLQRPGSDR corresponding to amino residues 775 to 790 at the N terminus of Megf8 (Aves Labs). The antibody was affinity purified and analyzed by ELISA. For immunostaining, cells were fixed in 4% paraformaldehyde at room temperature or embryos similarly fixed were cryoembedded and sectioned. Other primary antibodies used included goat anti-Gfi-1B (Clone D-19, 1:50; Santa Cruz), and mouse anti-SMARCD3 (1:100, clone 1G6; Abnova). Imaging was carried out using Zeiss LSM 510 META confocal microscope or a Leica DMRE microscope. Images were deconvolved using Openlab and Volocity imaging software.

Western Blot Analysis. A Megf8 fusion construct was generated by adding a 3XFLAG tag to the C terminus of full length Megf8 (GenBank accession no. EU723517) in p3XFLAG-CMV-14 expression vector (Sigma). NIH 3T3 cells transfected with this construct were lysed in RIPA buffer with 1% protease inhibitor mixture (Sigma P8340). Electrophoresis was carried out on 4–12% polyacrylamide NuPAGE Bis-Tris denaturing gels (Invitrogen) under reducing conditions. Proteins were transferred to nitrocellulose membranes and immunodetected using the Odyssey Infrared Imaging System (LI-COR Biosciences). Primary antibodies included chicken anti-Megf8 (1:5000, Aves Labs) and mouse anti-FLAG M2 (1:1,000; Sigma), with detection carried out using secondary antibodies: goat anti-mouse IgG IR700dx (1:10,000, Rockland) and goat anti-chicken IgY IR800 (1:10,000, Rockland).

***Megf8* Knockdown.** For shRNA mediated knockdown, cells were transiently transfected with SureSilencing shRNA plasmids for mouse *Megf8* containing a GFP reporter (SABiosciences) using Lipofectamine LTX (Invitrogen). The insert sequences were: 1, ACAGGCTACACCATGGACAAT; 2, TCACCGCCTGGGACATACTAT; 3, CTAGGTTGGTGTGTGCACAAT; 4, ACCCTTGAGCCCACAGAAGAT; and scrambled sequence control, GGAATCTCATTCGATGCATAC. Cells were fixed and examined after Megf8 antibody staining at 24 to 48 h after transfection.

ACKNOWLEDGMENTS. We thank Blake Carrington for technical support, Drs. Stuart H. Orkin and Yuko Fujiwara (Dana Farber Cancer Institute, Boston, MA) for providing *Gfi1b* knockout embryos, and Drs. Michael Shen (Columbia University Medical Center, New York) and Brent McCright (Center for Biologics Evaluation and Research, U.S. Food and Drug Administration, Bethesda, MD) for providing in situ hybridization probes. This work was supported by National Institutes of Health grants (to C.L, and P.J.D.J.), and Department of Energy Contract DE-AC02-05CH11231 (to L.A.P.).

1. Nusslein-Volhard C, Wieschaus E (1980) Mutations affecting segment number and polarity in Drosophila. *Nature* 287:795–801.
2. Shen Y, *et al.* (2005) Cardiovascular phenotyping of fetal mice by noninvasive high-frequency ultrasound facilitates recovery of ENU-induced mutations causing congenital cardiac and extracardiac defects. *Physiol Genomics* 24:23–36.
3. Yu Q, *et al.* (2004) ENU induced mutations causing congenital cardiovascular anomalies. *Development* 131:6211–6223.
4. Braslavsky I, Hebert B, Kartalov E, Quake SR (2003) Sequence information can be obtained from single DNA molecules. *Proc Natl Acad Sci USA* 100:3960–3964.
5. Margulies M, *et al.* (2005) Genome sequencing in microfabricated high-density picolitre reactors. *Nature* 437:376–380.
6. Shendure J, *et al.* (2005) Accurate multiplex polony sequencing of an evolved bacterial genome. *Science* 309:1728–1732.
7. Goldberg SM, *et al.* (2006) A Sanger/pyrosequencing hybrid approach for the generation of high-quality draft assemblies of marine microbial genomes. *Proc Natl Acad Sci USA* 103:11240–11245.
8. Dahl F, *et al.* (2007) Multigene amplification and massively parallel sequencing for cancer mutation discovery. *Proc Natl Acad Sci USA* 104:9387–9392.
9. Torres TT, Metta M, Ottenwalder B, Schlotterer C (2008) Gene expression profiling by massively parallel sequencing. *Genome Res* 18:172–177.
10. Wang Z, *et al.* (2008) Combinatorial patterns of histone acetylations and methylations in the human genome. *Nat Genet* 40:897–903.
11. Aune CN, *et al.* (2008) Mouse model of heterotaxy with single ventricle spectrum of cardiac anomalies. *Pediatr Res* 63:9–14.
12. Schultz J, Milpetz F, Bork P, Ponting CP (1998) SMART, a simple modular architecture research tool: Identification of signaling domains. *Proc Natl Acad Sci USA* 95:5857–5864.
13. Shiratori H, Hamada H (2006) The left–right axis in the mouse: From origin to morphology. *Development* 133:2095–2104.
14. Nonaka S, *et al.* (1998) Randomization of left–right asymmetry due to loss of nodal cilia generating leftward flow of extraembryonic fluid in mice lacking KIF3B motor protein. *Cell* 95:829–837.
15. Brennan J, Norris DP, Robertson EJ (2002) Nodal activity in the node governs left–right asymmetry. *Genes Dev* 16:2339–2344.
16. Saijoh Y, Oki S, Ohishi S, Hamada H (2003) Left-right patterning of the mouse lateral plate requires nodal produced in the node. *Dev Biol* 256:160–172.
17. Tanaka C, Sakuma R, Nakamura T, Hamada H, Saijoh Y (2007) Long-range action of Nodal requires interaction with GDF1. *Genes Dev* 21:3272–3282.
18. Gaio U, *et al.* (1999) A role of the cryptic gene in the correct establishment of the left–right axis. *Curr Biol* 9:1339–1342.
19. Lim J, *et al.* (2006) A protein–protein interaction network for human inherited ataxias and disorders of Purkinje cell degeneration. *Cell* 125:801–814.
20. Saleque S, Cameron S, Orkin SH (2002) The zinc-finger proto-oncogene Gfi-1b is essential for development of the erythroid and megakaryocytic lineages. *Genes Dev* 16:301–306.
21. Vassen L, Fiolka K, Moroy T (2006) Gfi1b alters histone methylation at target gene promoters and sites of gamma-satellite containing heterochromatin. *EMBO J* 25:2409–2419.
22. Takeuchi JK, *et al.* (2007) Baf60c is a nuclear Notch signaling component required for the establishment of left–right asymmetry. *Proc Natl Acad Sci USA* 104:846–851.
23. Quwailid MM, *et al.* (2004) A gene-driven ENU-based approach to generating an allelic series in any gene. *Mamm Genome* 15:585–591.
24. Albert TJ, *et al.* (2007) Direct selection of human genomic loci by microarray hybridization. *Nat Methods* 4:903–905.
25. Hodges E, *et al.* (2007) Genome-wide in situ exon capture for selective resequencing. *Nat Genet* 39:1522–1527.
26. Eid J, *et al.* (2009) Real-time DNA Sequencing from single polymerase molecues. *Science* 323:133–138.
27. Hirokawa N, Tanaka Y, Okada Y, Takeda S (2006) Nodal flow and the generation of left–right asymmetry. *Cell* 125:33–45.
28. Concha ML, Burdine RD, Russell C, Schier AF, Wilson SW (2000) A nodal signaling pathway regulates the laterality of neuroanatomical asymmetries in the zebrafish forebrain. *Neuron* 28:399–409.
29. Pennekamp P, *et al* (2002) The ion channel polycystin-2 is required for left–right axis determination in mice. *Curr Biol* 12:938–943.
30. Oki S, *et al.* (2007) *Development* 134:3893–3904.
31. Osoegawa K, de Jong PJ (2004) *Methods Mol Biol* 255:1–46.
32. Albrecht U, Eichele G, Helms J, Lu HC (1997) in Molecular and Cellular *Methods in Developmental Toxicology*, ed. Daston GP (CRC Press, New York), pp 23–48.